The International Journal of Advanced Manufacturing Technology (2022) 119:1035–1045
https://doi.org/10.1007/s00170-021-08333-3

ORIGINAL ARTICLE

Optimization solution of vertical rolling force using unified yield criterion

Yufeng Zhang[1,2] · Meiying Zhao[2] · Li Xu[1,2] · Hongshuang Di[1,2] · Xiaojuan Zhou[3] · Peng Wen[1,2] · Dewen Zhao[1,2] · Dianhua Zhang[1,2]

Received: 16 May 2021 / Accepted: 1 November 2021 / Published online: 13 November 2021

Abstract

Vertical rolling is an important technique used to control the width of continuous casting slabs in the hot-rolling field. Accurate prediction of vertical rolling force is a core point maintaining rolling-mill equipment. Owing to the limitation of the algorithm in use, the prediction accuracy of most vertical rolling force models based on the energy method can only reach more than 10%. Therefore, it is challenging to optimize the rolling-force model to improve prediction accuracy. An innovative approach for optimizing the calculation of vertical rolling force with a unified yield criterion is presented in this paper. First, the maximal width of a dog-bone region is determined by the slip-line method, and the dog-bone shape is described using a sine-function model. Second, the velocity and corresponding strain-rate fields satisfying kinematically admissible conditions are proposed to calculate the total power of the vertical rolling process. Finally, the analytical solution of the rolling force and the dog-bone-shape model is obtained by repeatedly optimizing the weighted coefficient b of intermediate principal shear stress on the yield criterion. Moreover, the effectiveness of the proposed mechanical model is verified by measured data in the strip hot-rolling field and other models' results. Results show that the prediction accuracy of the vertical rolling force model can be improved by optimizing the value of b. Then, the impacts of reduction rate, initial thickness, and friction factor on dog-bone shape size and vertical rolling force are discussed.

Keywords Vertical rolling force · Slip-line method · Dog-bone shape · Unified yield criterion

Abbreviations

W_0, W_E	Half of the initial and final slab width
W_x	Half of the slab width
ΔW	Unilateral reduction,$\Delta W=W_0-W_E$
ΔW_x	Unilateral reduction in deformation zone, $\Delta W_x=W_0-W_x$
h_0	Half of the initial slab thickness
h_{I}, h_{II}	Half of the slab thickness in zones I and II
h_p	Peak height of deformation zone
h_r	Edge height of deformation zone
R	Radius of edge roll
l	Projected length of contact arc, $l=\sqrt{2R\Delta W}$
v_0	Entrance velocity
v_{R}	Peripheral velocity of edge roll
θ	Bite angle, $\theta=\sin^{-1}(l/R)$
φ	Contact angle
d_0	The maximum width of dog bone region
d_φ	Deformation zone's width during edge rolling
d_{E}	Deformation zone's width after edge rolling
β	Undetermined parameters
b	Yield criterion parameter
v_x, v_y, v_z	Components of velocity vector
J^*	Total power
$\dot{W}_i$	Internal plastic deformation power
$\dot{W}_f$	Friction power
$\dot{W}_s$	Shear power
σ_s	Material yield stress
k	Yield shear stress, $k=\sigma_s/\sqrt{3}$
m	Friction factor
$J^*_{\min}$	Minimum value of total power
τ_f	Friction stress

✉ Hongshuang Di
dhshuang@mail.neu.edu.cn

[1] The State Key Laboratory of Rolling and Automation, Northeastern University, Shenyang 110819, Liaoning, People's Republic of China

[2] School of Materials Science and Engineering, Northeastern University, Shenyang 110819, Liaoning, People's Republic of China

[3] Ordos Institute of Applied Technology, Ordos 017000, Inner Mongolia, People's Republic of China

M	Rolling torque
ω	Roll angular velocity
$\overline{P}$	Rolling force
n_σ	Stress state coefficient
X	Arm coefficient
x, y, z	The directions of length, width, and thickness

1 Introduction

With the development of rolling technology, continuous casting and rolling have been extensively applied in many iron and steel enterprises. The width accuracy of hot-rolled strip steel products is an extremely important technical indicator in continuous casting and rolling processes. At present, the task of controlling the width of continuously cast slabs is mainly undertaken by vertical rolling and a sizing press (SP), and the reduction of vertical rolling is much smaller than that of the SP process. Owing to a small reduction and high width-to-thickness ratio, plastic deformation is concentrated on a tiny edge zone of the slab and presents an obvious dog bone shape after vertical rolling [1], as shown in Fig. 1. The dog-bone shape has a significant influence on the width spread of the subsequent flat rolling process and cannot be measured online, so the accurate prediction of dog-bone shape and rolling force is of enormous significance to automatic control.

Okado et al. [2], Toaze et al. [3], and Shibahara et al. [4] investigated the dog-bone shape by simulating the vertical-rolling process with pure lead and obtained a series of empirical formulas. Ginzburg et al. [5] modified Toaze's formulas and drew the conclusion that the relative dog-bone peak height increased with increasing reduction and decreased with increasing initial slab thickness. Xiong et al. [6, 7] obtained an experiential model of dog-bone shape after vertical rolling through physical simulation experiments on a laboratory rolling mill. However, these formulas can only describe the shape of the exit deformation zone, and prediction accuracy is affected considerably by different rolling conditions.

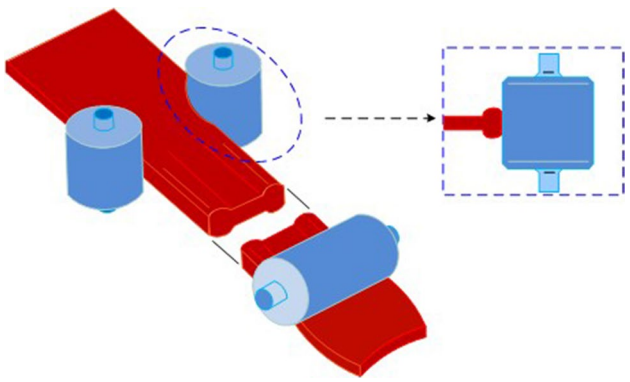

Fig. 1 Vertical-horizontal rolling in roughing mill and dog-bone shape

The finite element method (FEM) has been one of the best ways to analyze vertical rolling because it is suitable for solving intricate geometric deformation. Huisman and Huetink [8] investigated the effect of different vertical roll radii on the dog-bone shape after vertical rolling and verified the FEM results using plasticine as the experimental material. Chuang et al. [9] considered the geometric and material nonlinearities and established three-dimensional (3D) vertical-rolling and subsequent flat-rolling models based on the explicit dynamic equations by using the dynamic relaxation method, and obtained shape parameter data of the dog bone after edge rolling. Using the ABAQUS Explicit Solver, Forouzan et al. [10] proposed a 3D elastic-viscoplastic FEM model for vertical-rolling, studied the characteristics of geometric shape change and deformation law, and compared it with the SP. Ruan et al. [11] set up a 3D rigid-plastic FEM model with DEFORM to discuss the displacement velocity field of the deformation zone and the distribution of the dog-bone shape under different technological rolling parameters. Nevertheless, although the results obtained by the use of a FEM have high accuracy, a FEM cannot be used for online automatic control in practical production due to a large amount of computation time required.

In relation to the development of the analytical solution of vertical rolling force and a dog bone shape model, Yun et al. [12] proposed a mathematical model consisting of exponential and quartic functions, but the parameters of the dog-bone shape and vertical-rolling force were obtained by fitting FEM simulation data. Since the model did not offer the expression of the deformation power functional, Yun did not obtain the analytical solution of the vertical-rolling process. The present author previously proposed a method for calculating the vertical rolling force and dog-bone shape by combining a slip line and exponential velocity field [13]. Unfortunately, although an accurate prediction of the maximum width of the dog bone region, the error in calculating vertical-rolling force is slightly larger due to the selection of the upper-bound method, and the proposed dog-bone shape model is somewhat rough.

The unified yield (UY) criterion was proposed by Yu after noticing the nonlinearity of Mises's yield criterion, which is not a single yield criterion but a series of continuously variable linear yield criteria [14]. Then, Zhao et al. deduced the linear plastic work rate per unit volume of the UY criterion by a flow rule [15]. Therefore, herein, for the purpose of improving the prediction accuracy of edge rolling force, a new mathematical model is proposed by the energy method with the UY criterion, and the calculated accuracy of vertical rolling force is further improved by optimizing the weight coefficient in the UY criterion. Finally, the calculated

shape and mechanical parameters are verified, and the variation law of the stress-state coefficient under different rolling conditions is discussed.

2 Optimization of sine function dog bone shape model

In the vertical rolling process, owing to the large width-to-thickness ratio of the slabs, the plastic deformation is mainly restricted in a small area on the slab edge [12]. Therefore, the vertical rolling process can be approximately regarded as a plane deformation process and is suitable to be solved by the slip-line method.

As shown in Fig. 2, the maximum depth of the dog-bone region has been determined by the geometric characteristics of the vertical-rolling slip-line field in our previous study [16] and is expressed as follows:

$$d_0 = B'D' = BD = AB = 2h_0 \tag{1}$$

Based on Eq. (1), Liu's sine-function dog-bone-shape model was optimized [17], as shown in Fig. 3, and the mathematical expressions of half thickness $h(x, y)$ are the following:

Zone I: $(0 < y < W_E - d_E)$; half thickness h_I=$h_{II}(x, y)$ is

$$h_I = h_0 \tag{2}$$

Zone II: $(W_E - d_E < y < W_x)$; half thickness h_I=$h_{II}(x, y)$ is

$$h_{II} = h_0 + \beta\Delta W_x - \beta\Delta W_x \sin\left[\frac{3\pi\left(y - W_x\right)}{2d_\varphi}\right] \tag{3}$$

where β is an undetermined parameter, and on the basis of the incompressibility condition β=$\frac{3\pi h_0}{d_\varphi(2+3\pi)}$, W_x is half of the slab width, $W_x = R + W_E - \sqrt{R^2 - (l - x)^2}$.

The peak height of the deformation zone is

$$h_p = h_{II}\left(l, W_E - \frac{d_E}{3}\right) = h_0 + \frac{6\pi h_0 \Delta W}{d_E(2 + 3\pi)} \tag{4}$$

and its edge height is

$$h_r = h_{II}\left(l, W_E\right) = h_0 + \frac{3\pi h_0 \Delta W}{d_E(2 + 3\pi)} \tag{5}$$

where d_E is the width of the dog-bone zone after edge rolling, d_E=$d_0 - \Delta W$=$2h_0 - \Delta W$.

3 Velocity and strain rate fields

$dc - dC$ is the lateral variation of an infinitesimal segment in the direction of length, and $w = w(x, y)$ is the lateral displacement as shown in Fig. 3.

$$\frac{dw}{dy} = \frac{dc - dC}{dC} \tag{6}$$

The half-thickness is $h = h(x, y)$, and considering the incompressibility condition, the velocity of the rolling direction is

$$v_x = \frac{v_0 h_0}{h}\frac{dC}{dc} \tag{7}$$

Substituting Eq. (7) into Eq. (6) and noting that $\frac{dw}{dy} \ll 1$ and $\frac{dw/dy}{1+dw/dy} \approx \frac{dw}{dy}$, then

$$v_x = \frac{v_0 h_0}{h}\left(1 - \frac{dw}{dy}\right) \tag{8}$$

According to the properties of stream function

$$\frac{v_y}{v_x} = \frac{dw}{dx} \tag{9}$$

Substituting Eq. (8) into Eq. (9), the metal flow velocity of the width direction is derived as follows:

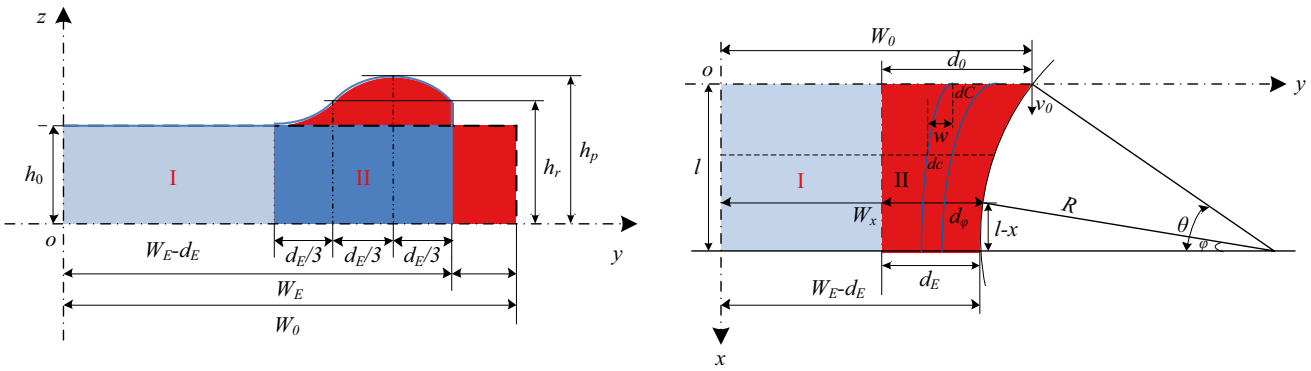

Fig. 2 Slip-line field and hodograph for edge rolling

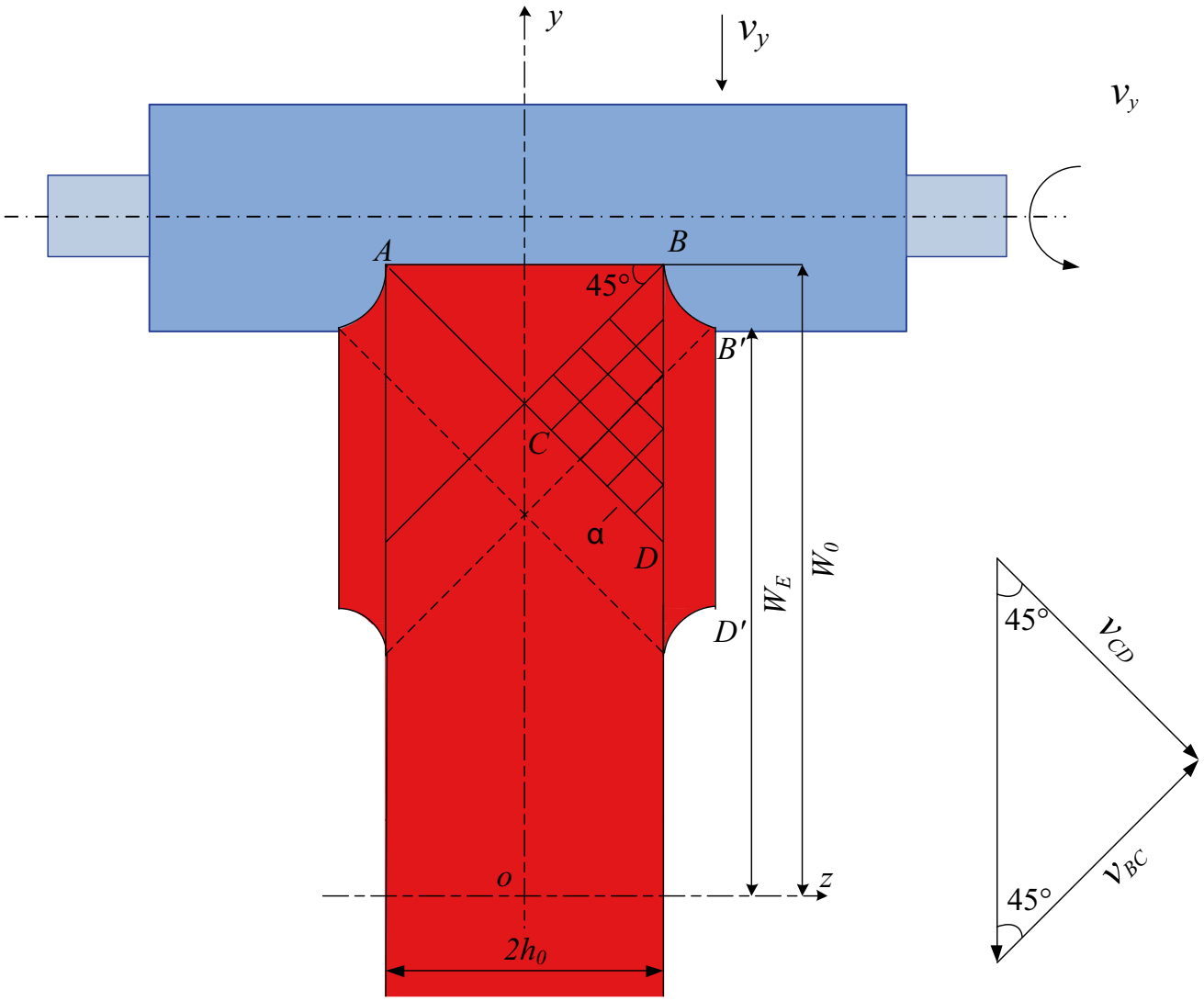

Fig. 3 Definition sketch of **a** sine-function dog-bone profile and **b** bite zone in vertical rolling

$$v_y = \frac{v_0 h_0}{h}\left(1 - \frac{\partial w}{\partial y}\right)\frac{\partial w}{\partial x} \tag{10}$$

Based on the plane-deformation assumption,

$$v_x = v_0 \tag{11}$$

Then in accordance with the incompressibility condition,

$$\begin{aligned}\dot{\varepsilon}_z &= -\left(\dot{\varepsilon}_x + \dot{\varepsilon}_y\right) = -\left(\frac{\partial v_x}{\partial x} + \frac{\partial v_y}{\partial y}\right)\\ &= v_0 h_0\left\{\frac{\partial}{\partial y}\left(\frac{1}{h}\right)\left[\frac{\partial w}{\partial x}\left(\frac{\partial w}{\partial y} - 1\right)\right] + \frac{1}{h}\frac{\partial^2 w}{\partial x \partial y}\left(\frac{\partial w}{\partial y} - 1\right) + \frac{1}{h}\frac{\partial}{\partial w}\frac{\partial^2 w}{\partial y^2}\right\}\end{aligned} \tag{12}$$

Noting that when $z = 0$, $v_z = 0$, the metal flow velocity of the vertical direction, v_z can be obtained by integrating $\dot{\varepsilon}_z$:

$$\begin{aligned}v_z &= \int \dot{\varepsilon}_y dy\\ &= v_0 h_0 z\left\{\frac{\partial}{\partial y}\left(\frac{1}{h}\right)\left[\frac{\partial w}{\partial x}\left(\frac{\partial w}{\partial y} - 1\right)\right] + \frac{1}{h}\frac{\partial^2 w}{\partial x \partial y}\left(\frac{\partial w}{\partial y} - 1\right) + \frac{1}{h}\frac{\partial}{\partial w}\frac{\partial^2 w}{\partial y^2}\right\}\end{aligned} \tag{13}$$

From Eqs. (8) and (11):

$$w = w(x, y) = \int_0^y \left(1 - h/h_0\right)dy \tag{14}$$

From Eqs. (2), (3), and (14), and the boundary conditions, the lateral displacement of each region can be obtained as follows:

Zone I:

$$w_I = \int_0^{W_E - d_E} \left(1 - h_I/h_0\right)dy = 0 \tag{15}$$

Zone II:

$$w_{II} = -\frac{3\pi\Delta W_x}{(2+3\pi)d_\varphi}\left[y-\left(W_x-d\varphi\right)\right]-\frac{2\Delta W_x}{2+3\pi}\cos\left[\frac{3\pi\left(y-W_x\right)}{2d_\varphi}\right] \tag{16}$$

It can be obtained from Eq. (16), $w_{II}\left(x,W_x\right)=-\Delta W_x$ and the boundary condition is satisfied.

Substituting Eq. (15) into Eqs. (10) and (13), the velocity field of zone I is derived as follows:

$$v_{xI}=v_0, v_{yI}=v_{zI}=0 \tag{17}$$

Then, the axial strain-rate field in zone I can be deduced on the basis of the Cauchy equation,

$$\dot{\varepsilon}_{xI}=\dot{\varepsilon}_{yI}=\dot{\varepsilon}_{zI}=0 \tag{18}$$

Inserting Eq. (16) into Eqs. (10) and (13), the velocity field of zone II is

$$\begin{aligned}
v_{xII}&=v_0\\
v_{yII}&=\frac{3\pi v_0\left(y-W_x+d_\varphi\right)}{(2+3\pi){d_\varphi}^2}\left[2h_0-\Delta W_x sin\left(\frac{3\pi\left(y-W_x\right)}{2d_\varphi}\right)\right]\frac{\mathrm{d}W_x}{\mathrm{d}x}+\frac{2v_0}{2+3\pi}\cos\left(\frac{3\pi\left(y-W_x\right)}{2d_\varphi}\right)\frac{\mathrm{d}W_x}{\mathrm{d}x}\\
v_{zII}&=-\frac{\pi v_0 z}{(2+3\pi)}\left\{\frac{6h_0}{{d_\varphi}^2}\left[1-sin\left(\frac{3\pi\left(y-W_x\right)}{2d_\varphi}\right)\right]-\frac{9\pi\left(y-W_x+d_\varphi\right)\Delta W_x}{2{d_\varphi}^3}\cos\left(\frac{3\pi\left(y-W_x\right)}{2d_\varphi}\right)\right\}\frac{\mathrm{d}W_x}{\mathrm{d}x}
\end{aligned} \tag{19}$$

From Eqs. (17) and (19), $v_{zI}\big|_{\substack{x=0\\z=0}}=v_{zII}\big|_{\substack{x=0\\z=0}}=0$, $v_{yII}\big|_{\substack{x=l\\y=W_E-d_E}}=0$, $v_{zI}\big|_{\substack{x=l\\z=0}}=v_{zII}\big|_{\substack{x=l\\z=0}}=0$, $v_{zI}\big|_{\substack{x=l\\z=h}}=v_{zII}\big|_{\substack{x=l\\z=h}}=0$, $v_{xI}\big|_{y=W_E-d_E}=v_{xII}\big|_{y=W_E-d_E}=v_0$, $v_{yI}\big|_{y=W_E-d_E}=v_{yII}\big|_{y=W_E-d_E}=0$, and $v_{zI}\big|_{y=W_E-d_E}=v_{zII}\big|_{y=W_E-d_E}=0$. These equations satisfy the boundary conditions.

Based on the Cauchy equation, the axial strain rate field in zone II is determined as follows:

$$\begin{aligned}
\dot{\varepsilon}_{xII}&=0\\
\dot{\varepsilon}_{yII}&=\frac{\pi v_0}{(2+3\pi)}\left\{\frac{6h_0}{d_\varphi^2}\left[1-sin\left(\frac{3\pi\left(y-W_x\right)}{2d_\varphi}\right)\right]-\frac{9\pi\left(y-W_x+d_\varphi\right)\Delta w_x}{2d_\varphi^3}\cos\left(\frac{3\pi\left(y-W_x\right)}{2d_\varphi}\right)\right\}\frac{\mathrm{d}W_x}{\mathrm{d}x}\\
\dot{\varepsilon}_{zII}&=-\frac{\pi v_0}{(2+3\pi)}\left\{\frac{6h_0}{d_\varphi^2}\left[1-sin\left(\frac{3\pi\left(y-W_x\right)}{2d_\varphi}\right)\right]-\frac{9\pi\left(y-W_x+d_\varphi\right)\Delta W_x}{2d_\varphi^3}\cos\left(\frac{3\pi\left(y-W_x\right)}{2d_\varphi}\right)\right\}\frac{\mathrm{d}W_x}{\mathrm{d}x}
\end{aligned} \tag{20}$$

From Eqs. (18) and (20), $\dot{\varepsilon}_{xI}+\dot{\varepsilon}_{yI}+\dot{\varepsilon}_{zI}=0$ and $\dot{\varepsilon}_{xII}+\dot{\varepsilon}_{yII}+\dot{\varepsilon}_{zII}=0$.

Thus, Eqs. (19) and (20) are the kinematically admissible velocity and strain-rate field, respectively.

4 Total power functional

4.1 UY criterion

The UY criterion is a unified expression of various linear yield criteria in the error triangle between Tresca's and the twin shear stress (TSS) yield loci on the π plane [14], as shown in Fig. 4.

Through an in-depth study, it is found that the UY yield criterion is more generalized than other linear yield criteria that have exact physical significance. The UY criterion is usually expressed by

$$\begin{cases}\sigma_1-\dfrac{b\sigma_2}{1+b}-\dfrac{\sigma_3}{1+b}=\sigma_s & \text{if } \sigma_2\le\frac{\sigma_1+\sigma_3}{2}\\ \dfrac{\sigma_1}{1+b}+\dfrac{b}{1+b}\sigma_2-\sigma_3=\sigma_s & \text{if } \sigma_2\ge\frac{\sigma_1+\sigma_3}{2}\end{cases} \tag{21}$$

where b is the yield-criterion parameter, which represents the effect of the intermediate principal shear stress on the yield of materials, and $0\le b\le 1$. σ_1, σ_2, and σ_3 are principal stresses.

The specific plastic work rate per unit volume of the UY criterion was derived by Zhao [15]

$$D\left(\varepsilon_{ij}\right)=\frac{1+b}{2+b}\sigma_s\left(\dot{\varepsilon}_{\max}-\dot{\varepsilon}_{\min}\right) \tag{22}$$

where $\dot{\varepsilon}_{\max}$ and $\dot{\varepsilon}_{\min}$ are the maximum and minimum strain rates, respectively, in deformation; $\dot{\varepsilon}_{\max}=\dot{\varepsilon}_z$ and $\dot{\varepsilon}_{\min}=\dot{\varepsilon}_y$.

When b takes any value between 0 and 1, the corresponding specific plastic power can be obtained. Zhao's research made considerable progress in the physical linearization of forming the energy-rate functional integral, which provides

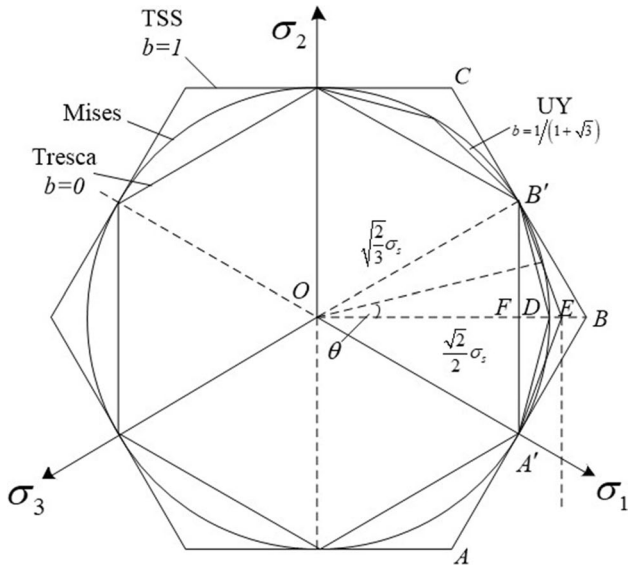

Fig. 4 Yield loci in π plane

a necessary basis for the first application of the UY criterion in this paper to improve the accuracy of the vertical-rolling force calculation by repeatedly optimizing the value of b in the UY yield criterion.

4.2 Inter-deformation power

Substituting Eqs. (18) and (20) into Eq. (22), the inter-deformation power can be calculated as follows:

$$\begin{aligned}\dot{W}_i &= \frac{4(1+b)}{2+b}\int_0^l\int_{W_E-d_E}^{W_x}\int_0^{h_I}\sigma_s\left(\dot{\varepsilon}_{\max}-\dot{\varepsilon}_{\min}\right)\mathrm{d}z\mathrm{d}y\mathrm{d}x\\ &= \frac{4(1+b)\sigma_s}{2+b}\int_0^l\int_{W_E-d_E}^{W_x}\int_0^{h_I}\left(\frac{-2\pi v_0}{(2+3\pi)}\left\{\frac{6h_0}{d_\varphi^2}\left[1-sin\left(\frac{3\pi(y-W_x)}{2d_\varphi}\right)\right]-\frac{9\pi(y-W_x+d_\varphi)\Delta W_x}{2d_\varphi^3}\cos\left(\frac{3\pi(y-W_x)}{2d_\varphi}\right)\right\}\frac{\mathrm{d}W_x}{\mathrm{d}x}\right)\mathrm{d}z\mathrm{d}y\mathrm{d}x\\ &= \frac{-4(1+b)\sigma_s}{2+b}\frac{\pi v_0 h_0}{(2+3\pi)}\int_{W_0}^{W_E}\left[\frac{(4+6\pi)h_0}{\pi d_\varphi}+\frac{(8+9\pi)h_0}{2+3\pi}\frac{3\Delta W_x}{d_\varphi^2}-\frac{(8+3\pi)}{4(2+3\pi)}\frac{3\Delta W_x^2}{d_\varphi^2}-\frac{2}{\pi}\frac{\Delta W_x}{d_\varphi}\right]dW_x\\ &= \frac{1+b}{2+b}\frac{3\sigma_s v_0 h_0}{(2+3\pi)^2(2h_0-\Delta W)}\left[16\pi(2h_0-\Delta W)h_0\ln\left(\frac{2h_0}{2h_0-\Delta W}\right)+\frac{4(2h_0-\Delta W)}{3}\left(4+6\pi+9\pi^2\right)\Delta W+(8+15\pi)\pi\Delta W^2\right]\end{aligned} \tag{23}$$

4.3 Friction power

Friction acts on the contact surface between the slab and vertical roll ($y = W_x$), and the tangential velocity discontinuity is

$$\Delta v_t = v_R - \frac{v_0}{\cos\varphi} \tag{24}$$

while the velocity discontinuity is

$$\Delta v_f = \sqrt{\left(v_{zII}\big|_{y=W_x}\right)^2+\Delta v_t^2} \tag{25}$$

It is noted that the friction stress $\tau_f = mk = m\sigma_s/\sqrt{3}$ and velocity discontinuity Δv_f are always in the same direction, and the friction power is then deduced using the collinear vector inner product

$$\begin{aligned}\dot{W}_f &= 4\int_0^l\int_0^{h_{rx}}|\tau_f||\Delta v_f|\cos(\Delta v_f,\tau_f)\mathrm{d}s\\ &= 4\int_0^l\int_0^{h_{rx}}\tau_f|\Delta v_f|\mathrm{d}s = 4mk\int_0^l\int_0^{h_{rx}}\sqrt{\left(v_{zII}\big|_{y=W_x}\right)^2+\Delta v_t^2}\frac{\mathrm{d}z\mathrm{d}x}{\cos\varphi}\end{aligned} \tag{26}$$

For the purpose of obtaining the analytical solution of the friction power, the mean-value theorem of the integral is used to calculate the average value of Δv_t,h_r, and v_{zII}:

$$\Delta\bar{v}_t = \frac{\int_\theta^0\left(v_R-\frac{v_0}{\cos\varphi}\right)\mathrm{d}\varphi}{-\theta} = v_R-\frac{v_0}{2\theta}\ln\left(\frac{R+l}{R-l}\right) \tag{27}$$

$$\bar{h}_r = \frac{h_{rl}+h_0}{2} = h_0+\frac{3\pi h_0\Delta W}{2(2+3\pi)(2h_0-\Delta W)} \tag{28}$$

$$\begin{aligned}\bar{v}_{zII} &= \frac{1}{l\bar{h}_r}\int_0^l\int_0^{\bar{h}_r}\left(v_{zII}\big|_{y=W_x}\right)\mathrm{d}z\mathrm{d}x = \frac{\pi v_0\bar{h}_r}{4(2+3\pi)l}\\ &\left[9\pi\ln\left(\frac{2h_0}{2h_0-\Delta W}\right)+\frac{3(3\pi-2)\Delta W}{2h_0-\Delta W}\right]\end{aligned} \tag{29}$$

Substituting $\mathrm{d}s = \frac{\mathrm{d}x\mathrm{d}y}{\cos\varphi}$ and $\mathrm{d}x = -R\cos\varphi\mathrm{d}\varphi$ into Eq. (26),

$$\begin{aligned}\dot{W}_f &= 4\int_0^l\int_0^{h_{rx}}\tau_f|\Delta v_f|\mathrm{d}s = 4\int_0^l\int_0^{h_{rx}}|\tau_f||\Delta v_f|\cos(\Delta v_f,\tau_f)\mathrm{d}s\\ &= 4\int_0^l\int_0^{h_{rx}}\Delta v_f\tau_f\mathrm{d}s = \frac{4m\sigma_s\bar{h}_rR\theta}{\sqrt{3}}\left\{\Delta\bar{v}_t\left[1+\left(\bar{v}_{zII}/\Delta\bar{v}_t\right)^2\right]^{-1/2}\right.\\ &\left.+\bar{v}_{zII}\left[1+\left(\Delta\bar{v}_t/\bar{v}_{zII}\right)^2\right]^{-1/2}\right\}\end{aligned} \tag{30}$$

4.4 Shear power

On the basis of the mean value theorem, the velocity field in the transverse region of the entrance becomes the following:

Zone I:

$$\bar{v}_{yI}=\bar{v}_{zI}=0 \tag{31}$$

Zone II:

$$\begin{aligned}\bar{v}_{yII}&=-\frac{3v_0\tan\theta}{2(2+3\pi)h_0}\frac{\int_{W_0-2h_0}^{W_0}\left[\pi\left(y-W_0+2h_0\right)+\frac{4}{3}h_0\cos\left(\frac{3\pi(y-W_0)}{4h_0}\right)\right]\mathrm{d}y}{2h_0}\\&=-\frac{\tan\theta v_0\left(9\pi^2-8\right)}{6\pi(2+3\pi)}\quad \bar{v}_{zII}=\frac{3\pi\tan\theta v_0 z}{2(2+3\pi)h_0}\frac{\int_{W_0-2h_0}^{W_0}\left[1-sin\left(\frac{3\pi(y-W_0)}{4h_0}\right)\right]\mathrm{d}y}{2h_0}\\&=\frac{\tan\theta v_0 z}{2h_0}\end{aligned} \tag{32}$$

The shear power can then be expressed as

$$\begin{aligned}\dot{W}_s&=4k\int_{W_0-2h_0}^{W_0}\int_0^{h_0}\sqrt{(\bar{v}_{yII})^2+(\bar{v}_{zII})^2}\mathrm{d}z\mathrm{d}y\\&=\frac{4k\tan\theta v_0}{2h_0}\int_{W_0-2h_0}^{W_0}\int_0^{h_0}\sqrt{z^2+\left[\frac{9\pi^2-8}{3\pi(2+3\pi)}h_0\right]^2}\mathrm{d}z\mathrm{d}y\\&=\frac{2\sigma_s\tan\theta v_0 h_0^2}{\sqrt{3}}\left[\sqrt{1+\left[\frac{9\pi^2-8}{3\pi(2+3\pi)}\right]^2}+\left[\frac{9\pi^2-8}{3\pi(2+3\pi)}\right]^2\right.\\&\quad\left.\ln\frac{1+\sqrt{1+\left[(9\pi^2-8)/3\pi(2+3\pi)\right]^2}}{(9\pi^2-8)/3\pi(2+3\pi)}\right]\end{aligned} \tag{33}$$

4.5 Total power and its optimization

Substituting Eqs. (23), (30), and (33) into $J^*=\dot{W}_i+\dot{W}_f+\dot{W}_s$ yields the analytical solution of the total power functional

$$\begin{aligned}J^*=&\frac{1+b}{2+b}\frac{3\sigma_s v_R h_0\cos\theta}{(2+3\pi)^2(2h_0-\Delta W)}\left[16\pi(2h_0-\Delta W)h_0\ln\left(\frac{2h_0}{2h_0-\Delta W}\right)\right.\\&\left.+\frac{4(2h_0-\Delta W)}{3}(4+6\pi+9\pi^2)\Delta W+(8+15\pi)\pi\Delta W^2\right]\\&+\frac{4m\sigma_s\bar{h}_r R\theta}{\sqrt{3}}\left\{\Delta\bar{v}_t\left[1+\left(\bar{v}_{zII}/\Delta\bar{v}_t\right)^2\right]^{-1/2}+\bar{v}_{zII}\left[1+\left(\Delta\bar{v}_t/\bar{v}_{zII}\right)^2\right]^{-1/2}\right\}\\&+\frac{2\sigma_s\tan\theta v_0 h_0^2}{\sqrt{3}}\left[\sqrt{1+\left[\frac{9\pi^2-8}{3\pi(2+3\pi)}\right]^2}+\left[\frac{9\pi^2-8}{3\pi(2+3\pi)}\right]^2\ln\frac{1+\sqrt{1+\left[(9\pi^2-8)/3\pi(2+3\pi)\right]^2}}{(9\pi^2-8)/3\pi(2+3\pi)}\right]\end{aligned} \tag{34}$$

J^* is only relevant to the yield criterion parameter b when the deformation resistance σ_s, reduction ΔW, radius of edge roll R, peripheral velocities v_R, initial thickness of slabs $2h_0$, and friction factor of edge roll-slab arc m are given. Therefore, the value of b can be repeatedly optimized between 0 and 1 according to the measured vertical rolling force data to improve the accuracy of Eq. (34). Then, the corresponding values of rolling torque M, rolling force $\bar{P}$, and stress state coefficient n_σ can be achieved separately as follows [18]:

$$M=\frac{J^*}{2\omega},\ \bar{P}=\frac{M}{\chi l},\ n_\sigma=\frac{\bar{P}}{\sigma_s} \tag{35}$$

The arm coefficient $\chi=0.3$–0.6 was researched in the hot-rolling process [19], and $\chi=0.5$ is selected in this paper under the relevant equipment and process parameters.

5 Results

5.1 Dog-bone shape

To verify the accuracy of the dog-bone-shape model proposed in this paper, the ratio of dog-bone peak height to width, h_p/W_0, was calculated by Eq. (4) under different engineering strains $\Delta W/W_0$, initial thicknesses h_0, and vertical-roll radii R. In addition, a comparison between the optimized sine-function-model results and those of other models is shown in Figs. 5 and 6. The comparison results demonstrate that the deviation between Eq. (4) and Ginzburg's model is within 5.7% and that between Eq. (4) and Xiong's model is within 8%. As can be seen from Fig. 5, the deflections between the present model and the other two models will increase with increasing reduction ΔW. When the value of $\Delta W/W_0$ is less than 0.015, the comparative deflections are reduced to 1.5% and 5%. Because the present model assumed that the edge rolling process

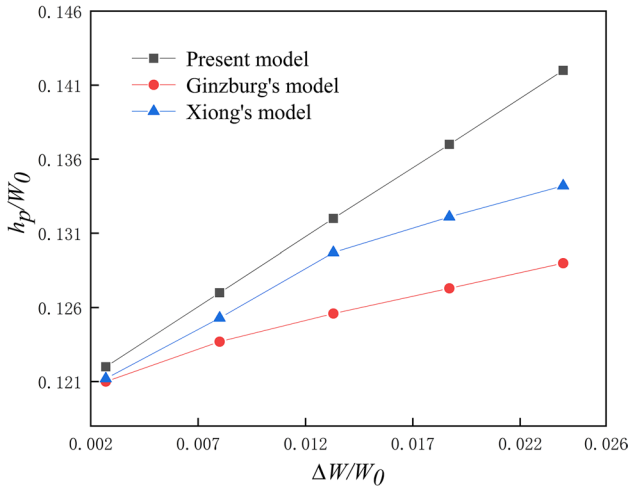

Fig. 5 Influence of $\Delta W/W_0$ on h_p/W_0

is a plane-deformation process, it is reasonable that the value of h_p/W_0 is higher than those of both Xiong's and Ginzburg's models.

5.2 Edge rolling force

To validate the vertical rolling force model proposed in this paper, the authors collected a large amount of actual measurement data in the hot rolling production line of a Chinese steel company. Its roughing mill group consists of two vertical roll stands and two horizontal rolling stands, and Fig. 7 shows its schematic diagram and main electrical characteristics.

Taking the material of Q235 steel product for instance, the cast slab with dimension of $180 \times 480 \times 7000$ (mm^3)

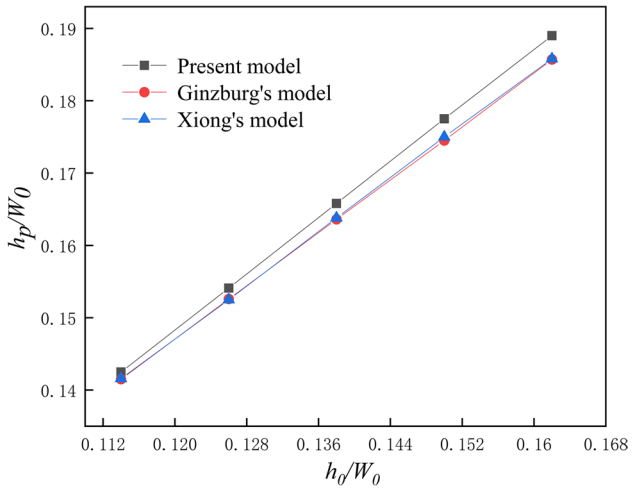

Fig. 6 Influence of h_0/W_0 on h_p/W_0

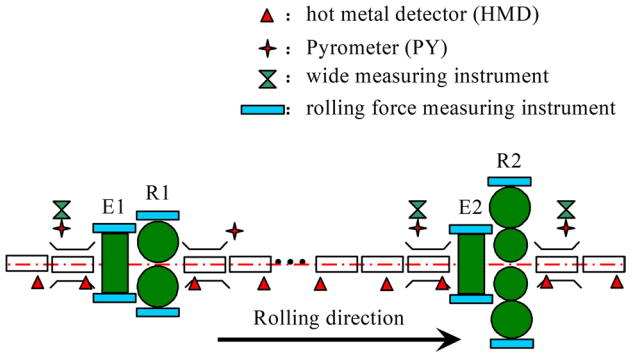

Fig. 7 Schematic diagram and main characteristics of the roughing mill group

is reduced from 480 to 455 mm by vertical roll stands E1 and E2 in the roughing mills. The radius of vertical roll, peripheral velocity v_R, temperature t, and true strain $\varepsilon = \ln\left(W_0/W_E\right)$ for vertical stands are shown in Table 1, and the deformation resistance of the slabs is also included. Then the rolling process parameters in Table 1 are substituted into Eqs. (33) and (34) to calculate the vertical-rolling force and compare with the rolling force values monitored by two force transducers located over the bearing blocks of the vertical roll. By repeatedly optimizing the value of b, the error between the calculated force and actual measured data is within 5% when $b = 0.613$, as shown in Table 1.

The model of deformation resistance for the Q235 steel used in the calculation is determined by Wang et al. [20], which can be expressed mathematically as

$$\sigma_s = \sigma_0 e^{(a_1 T - a_2)} \left(\frac{\dot{\varepsilon}}{10}\right)^{(a_3 T - a_4)} \left[a_6 \left(\frac{\varepsilon}{0.4}\right)^{a_5} - \left(a_6 - 1\right)\frac{\varepsilon}{0.4}\right] \tag{36}$$

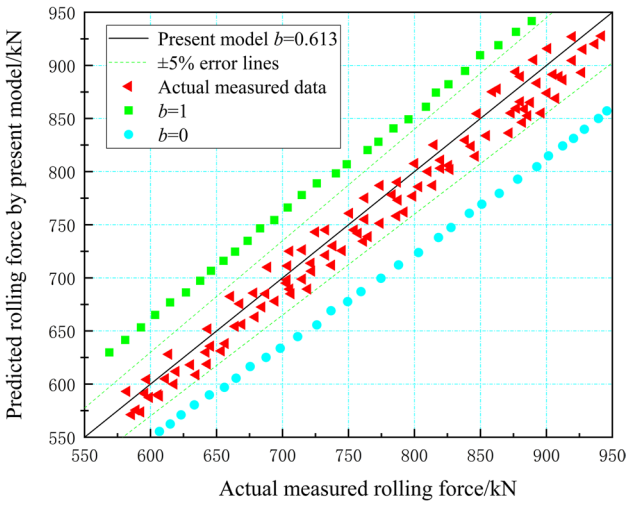

Fig. 8 Comparison between calculated rolling force under different b values and actual measured data

Table 1 Comparison of vertical rolling force calculated by present model with measured one

Stand no.	v_R (m/s)	t (℃)	$\varepsilon = \ln(W_0/W_E)$	σ_s (MPa)	R (m)	Calculated force (kN)	Measured force (kN)	Error (%)
E1	0.76	1139.3	0.032	35.24	0.55	968.09	922.87	4.9
E2	1.28	1114.7	0.021	32.17	0.542	874.39	838.34	4.3

where $\sigma_0 = 150$ MPa, $a_1 = -2.8685$, $a_2 = 3.6573$, $a_3 = 0.2121$, $a_4 = -0.1531$, $a_5 = 0.3912$, $a_6 = 1.4403$, $T=(t+273)/1000$.

In addition, the authors also used the TSS ($b = 1$) and the Tresca yield criteria ($b = 0$) for calculating the vertical-rolling force with a maximum error of 12% and 15%, as shown in Fig. 8. This indicates that the application of the UY criterion can effectively improve the accuracy of the vertical rolling-force calculation by the energy method.

6 Discussion

Based on the dog-bone-shape model, Eq. (4), and the vertical rolling-force model, Eqs. (33) and (34), proposed in the present paper, the influence of different rolling process parameters on dog-bone peak height h_p and vertical rolling force is studied, and the results are shown in Figs. 5 and 6 and in Figs. 9 and 10.

Figure 5 shows the significant increase in dog-bone peak height during the vertical rolling process with increasing engineering strain $\Delta W/W_0$. This is caused by the length of the contact arc and the volume of the deformed metal, increasing while ΔW increases. Since the plastic deformation is concentrated on the edge of the slab, h_p obviously increases. In Fig. 6, the dog-bone peak height h_p shows a linear growth trend with the increase of the slab's initial thickness h_0, which is consistent with Xiong's and Ginzburg's models. This is because, when only h_0 increases, the contact-arc length between the slab and vertical roll remains unchanged, but the contact surface of the rolling slab becomes larger, which increases the volume of metal involved in plastic deformation, resulting in an increase in the value of h_p. Furthermore, although h_p increases with h_0, the increase in h_p is much smaller than that in h_0, which is why the curves in Fig. 6 are linear.

The vertical rolling force is another key parameter studied in the present paper, and according to the calculation results shown in Fig. 8, it can be seen that the variation of the yield criterion parameter b has a drastic positive effect on the calculated value of the vertical rolling force. This is because the inter-deformation power accounts for a large proportion of the total power in the vertical rolling process. After optimizing the vertical rolling force model by adjusting the value of the yield criterion parameter b, the impact of slab thickness h_0 and reduction ΔW on the vertical rolling force is studied, and the results are shown in Fig. 9. Figure 9 shows that the stress-state coefficient n_σ increases significantly with increasing h_0/W_0 and engineering strain $\Delta W/W_0$, and the increasing trend of n_σ is from sharp to gentle as h_0/W_0 and $\Delta W/W_0$ increase. In addition, it is evident from Fig. 9 that the influence of engineering strain on the stress state coefficient is much greater than that of the initial thickness, and it is the main factor affecting the change of rolling force.

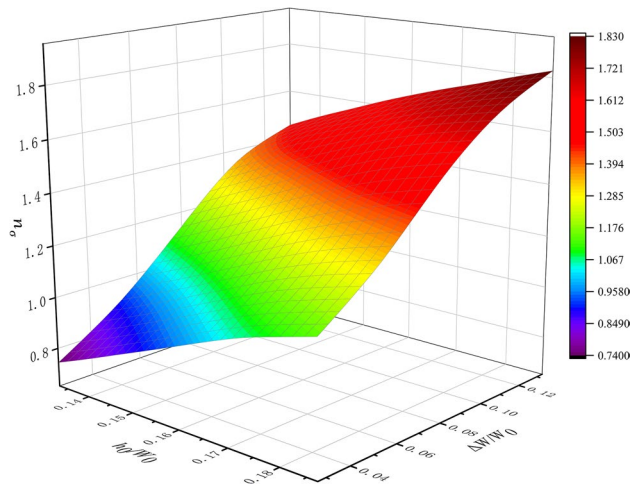

Fig. 9 Influence of $\Delta W/W_0$ and h_0/W_0 on stress state coefficient n_σ

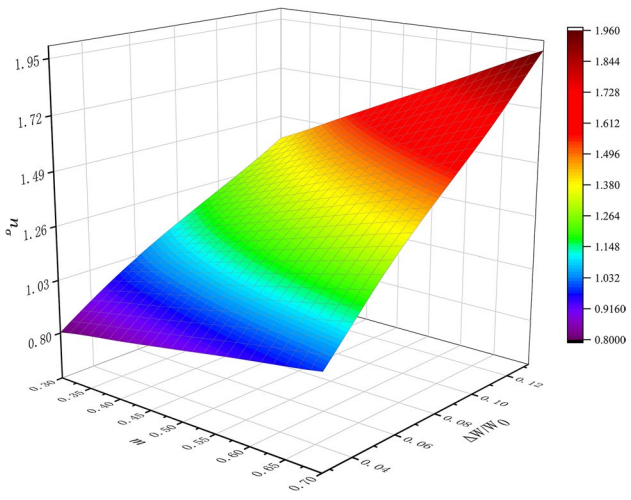

Fig. 10 Influence of $\Delta W/W_0$ and friction factor m on stress state coefficient n_σ

Figure 10 shows the influence law of friction coefficient m and $\Delta W/W_0$ on the influence coefficient of the stress state. When the engineering strain is small, the friction coefficient has little influence on the rolling force, but as the engineering strain becomes larger, the friction coefficient exhibits a rapid increase in the influence of the rolling force.

7 Conclusions

1. The UY criterion is first proposed establishing the vertical rolling force model, and the yield criterion parameter b is converted into an optimal parameter of the vertical rolling force. Then, the value of b is repeatedly optimized, and it is determined that the mechanical model in this paper achieves the highest accuracy when $b = 0.613$, the error between the optimized model calculation results and the field measured data is within 5%.
2. The vertical rolling forces calculated by UY, TSS, and Tresca yield criteria are compared with actual measured data. It is noted that the prediction accuracy of the rolling force is effectively improved by optimizing the yield parameter b. This proves that it is feasible and effective to use the UY criterion to optimize the solution accuracy of mechanical parameters.
3. The sine-function dog-bone-shape model is optimized by using the slip line field to determine the maximum depth of the dog bone area, which ensures the prediction accuracy and simplifies the calculation steps, which can improve the prediction efficiency of the slab shape after vertical rolling.
4. Engineering strain is the primary factor that affects the height of the bone peak of the dog bone shape. The increase of the initial thickness of the slab also increases the height of the bone peak, but it is far from the obvious influence of the engineering strain on the height of the bone peak. In addition, the increases of engineering strain, initial slab thickness, and friction coefficient will cause different degrees of increase in the rolling force. The co-increasing of engineering strain and friction coefficient will make the rolling force present the most obvious increasing trend.

Author contribution Yufeng Zhang wrote the first draft of the paper. All authors revised and approved the final version of the manuscript.

Funding This study was funded by the National Natural Science Foundation of China (No. U20A20187) and the National Key R&D Program of China (No. 2017YFB0304100).

Availability of data and materials The datasets used or analyzed during the current study are available from the corresponding author on reasonable request.

Declarations

Ethics approval Not applicable.

Consent to participate Not applicable.

Consent to publication Not applicable.

Competing interests The authors declare no competing interests.

References

1. Ginzburg VB (1989) Steel-rolling technology: theory and practice. Marcel Dekker, New York
2. Okado M, Ariizumi T, Noma Y, Yabuuchi K, Yamazaki Y (1981) Width behaviour of the head and tail of slabs in edge rolling in hot strip mills. Tetsu To Hagane 67:2516–2525. https://doi.org/10.2355/tetsutohagane1955.67.15_2516
3. Tazoe N, Honjyo H, Takeuchi M (1984) New forms of hot strip mill width rolling installations. AISE Spring Conference. Dearborn, USA, pp 85–88
4. Shibahara T, Misaka Y, Kono T, Koriki M, Takemoto H (1981) Edger set-up model at roughing train in a hot strip mill. Tetsu To Hagane 67:2509–2151. https://doi.org/10.2355/tetsutohagane1955.67.15_2509
5. Ginzburg VB, Kaplan N, Bakhtar F, Tabone CJ (1991) Width control in hot strip mills. Iron Steel Eng 68:25–39
6. Xiong SW, Zhu XL, Liu XH, Wang G, Zhang Q, Li H, Meng X, Han L (1997) Mathematical model of width reduction process of roughing trains of hot strip mills. Shanghai Metal 19(1):39–43
7. Xiong SW, Rodrigues JMC, Martins PAF (2003) Three-dimensional modelling of the vertical-horizontal rolling process. Finite Elem Anal Des 39:1023–1037. https://doi.org/10.1016/s0168-874x(02)00154-3
8. Huisman HJ, Huetink J (1985) A combined Eulerian-Lagrangian three-dimensional finite-element analysis of edge-rolling. J Mech Work Technol 11:333–353. https://doi.org/10.1016/0378-3804(85)90005-1
9. Chung WK, Choi SK, Thomson PF (1993) Three-dimensional simulation of the edge rolling process by the explicit finite-element method. J Mater Process Technol 38(1):85–101. https://doi.org/10.1016/0924-0136(93)90188-C
10. Forouzan MR, Salehi I, Adibi-sedeh AH (2009) A comparative study of slab deformation under heavy width reduction by sizing press and vertical rolling using FE analysis. J Mater Process Technol 209(2):728–736. https://doi.org/10.1016/j.jmatprotec.2008.02.063
11. Ruan JH, Zhang LW, Gu SD (2015) Finite element simulation based plate edging model for plan view pattern control during wide and heavy plate rolling. Ironmak Steelmak 41(3):199–205
12. Yun D, Lee D, Kim J, Hwang S (2012) A new model for the prediction of the dog-bone shape in steel mills. ISIJ Int 52:1109–1117. https://doi.org/10.2355/isijinternational.52.1109
13. Zhang YF, Di HS, Li X, Peng W, Zhao DW, Zhang DH (2020) A novel approach for the edge rolling force and dog-bone shape by combination of slip-line and exponent velocity field. SN Appl Sci 2:2055. https://doi.org/10.1007/s42452-020-03770-3
14. Yu MH, He LN, Liu CY (1992) Generalized twin-shear stress yield criterion and its generalization. Chinese Sci Bull 37(24):2085–2089. CNKI:SUN:JXTW.0.1992-24-013
15. Zhao DW, Li J, Liu XH, Wang GD (2009) Deduction of plastic work rate per unit volume for unified yield criterion and its application. Trans Nonferrous Met Soc China 19:657–660. https://doi.org/10.1016/S1003-6326(08)60329-5

16. Zhang YF, Zhang HY, Chen LJ, Zhao DW, Zhang DH (2018) Calculation of vertical rolling force through slip-line field. J Plast Eng 25:288–291. https://doi.org/10.3969/j.issn.1007-2012.2018.06.042
17. Liu YM, Ma GS, Zhang DH, Zhao DW (2015) Upper bound analysis of rolling force and dog-bone shape via sine function model in vertical rolling. J Mater Process Technol 223:91–97. https://doi.org/10.1016/j.jmatprotec.2015.03.051
18. Zhang SH, Wen HT, Lei D (2021) A novel yield criterion and its application to calculate the rolling force of a thick plate during hot rolling. J Braz Soc Mech Sci 43:12. https://doi.org/10.1007/s40430-020-02761-0
19. Zhang DH, Liu YM, Sun J, Zhao DW (2016) A novel analytical approach to predict rolling force in hot strip finish rolling based on cosine velocity field and equal area criterion. Int J Adv Manuf Tech 84:843–850. https://doi.org/10.1007/s00170-015-7692-z
20. Wang XH, Liu CY, Deng YC (2011) Model of deformation resistance of Q235 steel. Metall Inf Rev 1:25–30